Construction and Building Materials 420 (2024) 135582

Contents lists available at ScienceDirect

Construction and Building Materials

journal homepage: www.elsevier.com/locate/conbuildmat

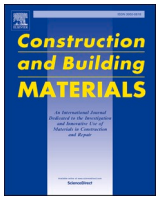

Mechanical and morphological variations of basalt fiber in seawater and a strategy to improve its performance with nanocomposite sizing

Meng Li [a,b,1], Hui Li [a,b,1], Ghizlane Achagri [a,b], Cun-Guang Liang [a,b], Molong Duan [c], Dan Xing [a,b,*], Peng-Cheng Ma [a,b,*]

[a] Laboratory of Environmental Science and Technology, The Xinjiang Technical Institute of Physics and Chemistry, Key Laboratory of Functional Materials and Devices for Special Environments, Chinese Academy of Sciences, Urumqi 830000, China
[b] Center of Materials Science and Optoelectronics Engineering, University of Chinese Academy of Sciences, Beijing 100049, China
[c] Department of Mechanical and Aerospace Engineering, The Hong Kong University of Science and Technology, the Hong Kong Special Administrative Region of China

ARTICLE INFO

Keywords:
Basalt fiber
Seawater erosion
Nanocomposite sizing
Corrosion resistance

ABSTRACT

Basalt fiber-reinforced polymers are expected as a promising candidate in the construction industry, especially in marine engineering. However, the study on the durability of basalt fiber (BF) exposed to seawater is still in its infancy. In this paper, the corrosion behavior of BF in seawater was discussed. The results manifested that the strength of BF generally increased and then reduced with accumulation of treatment temperature or duration in seawater. Notably, the tensile strength of BF increased by 22.5% in initial stage due to the Na^+/K^+ exchange between the fiber and seawater. As the interaction proceeded, multi-scale particles emerged on the fiber surface, followed by the formation of corrosion layer with different thickness. To address the problem caused by the seawater, nanocomposite sizing containing nanosheet was applied on BF surface, which could considerably enhance the mechanical and seawater-resistance performance of filament. In-depth analysis confirmed that such improvement originated from the synergetic effects of stress transfer and the barrier performance of nanosheet in nanocomposite sizing.

1. Introduction

With the exploration and utilization of marine resources, infrastructure construction in some coastal countries for the ports, seawalls, bridges, islands, and reefs has been booming in recent years. Given the erosion environment in seawater, the durability of building structures under such condition is a critical issue to be considered [1]. For example, steel bars in concrete are likely to be rusted because of the constant intrusion of multiple ions (Cl^-, SO_4^{2-}) from seawater [2]. In a saline environment, the erosion of seawater could cause damage and failure to the concrete, which will threaten the life span of the buildings, thus triggering safety accident and economic loss. Therefore, developing alternative materials with long durability in the seawater environment is of great importance.

Recently, steel bars in concrete have been replaced with polymers or fiber-reinforced polymers because of their lightweight, anti-fatigue, anti-corrosion, and easy processing [3–6]. For example, Lee et al. [7] introduced polyethylene terephthalate fibers and nano-SiO_2 to enhance the mechanical property of concrete. Notably, basalt fiber-reinforced polymer (BFRP), a cost-effective material, has attracted extensive attention to address these problems [8,9]. In BFRP, basalt fiber (BF) is employed as the reinforcement in the composites, which has the advantages of excellent mechanical property, environmentally friendly nature, and high working temperature [10]. Generally, the fiber breakage is considered to be responsible for the failure of BFRP under the static tension [11]. In the seawater, multiple ions can permeate the fiber-reinforced polymer and then erode the reinforcement, forming micro-cracks on the fiber surface. To improve the durability of the BFRP, in-depth understanding on the corrosion behavior of BF in the seawater is necessary.

Up to date, only a few studies have reported the corrosion behavior of BF under seawater environment. For example, Benmokrane et al. [12] found that the weight loss of BF reached 0.3% when the filament was immersed in 10% NaCl solution at 96 °C for 168 h. Pan and co-workers

* Corresponding authors at: Laboratory of Environmental Science and Technology, The Xinjiang Technical Institute of Physics and Chemistry, Key Laboratory of Functional Materials and Devices for Special Environments, Chinese Academy of Sciences, Urumqi 830000, China.
E-mail addresses: xingdan@ms.xjb.ac.cn (D. Xing), mapc@ms.xjb.ac.cn (P.-C. Ma).
[1] These authors contributed to this work equally.

https://doi.org/10.1016/j.conbuildmat.2024.135582
Received 22 December 2023; Received in revised form 28 January 2024; Accepted 21 February 2024
Available online 29 February 2024

[13] studied the durability of BF exposed to the simulated seawater at 20 °C, 40 °C and 60 °C for 90 days. The results demonstrated that the tensile strength of single fiber declined by 61% after 90 days at 60 °C. Most of the studies mainly focused on the variations in the mass and strength of fiber under single variables. For instance, Liu's group [14] studied the corrosion process of BF placed in seawater at 70 °C for 12 h, and they found that the mass and strength retention rates of fiber in seawater were above 92.73% and 70.54%, respectively. Furthermore, the elemental composition of BF after seawater treatment was investigated. The results showed that the presence of insoluble substances, such as Ca $(OH)_2$ and $Fe_2O_3{\cdot}nH_2O$, on the fiber surface, was beneficial to the corrosion resistance of fiber. From the reported literatures, it could be concluded that the progress achieved in this field mainly dealt with the role of OH^- in the seawater to destroy the fiber structure. The effect of multiple anions in seawater, including SO_4^{2-} and Cl^-, on the fiber structure was still obscure, which was expected to be essential to figure out the exact mechanism of BF corrosion in seawater.

With a rational understanding on the briny corrosion behavior of BF, efforts have been made to improve the corrosion resistance of BF, especially in the alkali conditions. The addition of alkali-resistant components, such as ZrO_2 [15], La_2O_3 [16], and TiO_2 [17], during the spinning of BF, could improve the alkali-resistant performance of the filament. However, the crystallization kinetics of BF were altered by adopting this method, which led to the formation of crystals in the amorphous fiber, definitely deteriorating the strength of the filament. In this context, the application of sizing on BF surface is an easy way to modulate the anti-corrosion performance of fiber. When formulating the sizing with various organic compounds, the hydrolysis of the mixture occurs, thus healing the micro-cracks on fiber surface and providing protection to the fiber [18]. Adding nanofiller into the sizing can slow down the penetration of the corrosive solution. For example, the introduction of the plate-like graphene in sizing obstructed the invasion of moisture and alkali ions, thus contributing to the anti-corrosion performance of glass fiber [19]. In another study, the presence of nanoclay in sizing prohibited the corrosive ions in water from approaching the glass fiber surface due to the tortuous and longer paths derived from the piling of the nanofiller [20].

Herein, the corrosion behavior of BF in seawater was studied, and the effects of treatment parameters (Immersion temperature and time) on the tensile strength and mass of BF were investigated. Variations on the microstructure of BF before and after treatment were compared, and the erosion mechanism was discussed with an emphasis on analyzing the interactions of various anions and cations between the fiber and seawater. Moreover, a functional sizing consisting of polysilsesquioxane nanosheet was prepared and applied on BF surface, and the seawater resistance of BF with this nanocomposite sizing was investigated.

2. Experimental setups

2.1. Materials

BF without sizing (Guizhou Shixin, China) was used in this work. Basic properties of BF were listed in Table 1 and Table 2, including the fiber diameter, tensile strength of bundle fibers and single fiber. The BF was mainly comprised of O, Si, Al, Fe and Ti, as well as alkaline (Na, K) and alkaline-earth (Ca, Mg) metals. Hexadecyltrimethoxysilane (HDTMS) was supplied by Double Peach Fine Chemical Co., Ltd (Guangzhou, China). Sodium hydroxide (NaOH), ethanol (EtOH), and glacial acetic acid were purchased from Baishi Chemical Industry Co., Ltd (Tianjin, China). The following agents were used for the preparation of sizing: Epoxy resin (E-51, Xingchen Synthetic Materials Co., Ltd, Nantong, China), Span-80 (Hedong Hongyan Reagent Factory, Tianjin, China), sodium dodecyl sulfate (SDS, Zhiyuan Chemical Reagent Co., Ltd, Tianjin, China), γ-aminopropyltriethoxysilane (KH-550, Yuanye Bio-Technology Co., Ltd, Shanghai, China), hexadecyltrimethylammonium bromide (CTAB, Yongsheng Fine Chemical Co., Ltd, Tianjin, China), polyethylene glycol monostearate (PEG-MS, Haian Petrochemical Factory, Nantong, China). All chemicals were used without further purification.

Table 1
Properties of basalt fiber.

Diameter (μm)	Yarn fineness (tex)	Density (g/cm^3)	Tensile strength of bundle fibers (N/tex)	Tensile strength of single fiber (MPa)
16.04 ±1.60	222.38 ±10.27	2.61 ±0.03	0.13±0.02	1324±333

2.2. Fiber treatment

The simulated seawater was prepared based on the standard (ASTM D1141–98). Bundles of BF (1.0 m, 0.2 g) were soaked in the simulated seawater (50.0 mL) at various temperature for different time according to the experimental schemes, as listed in Table 3 and Table 4. After the treatment, the sample was washed three times using water and dried at 105 °C for 1 h. The treated BF sample was labelled as A (Immersion temperature)-B (Immersion time).

2.3. Preparation of nanocomposite sizing

As schematically shown in Fig. 1A, the preparation of the nanocomposite sizing involved both the synthesis of nanofiller and formulation of epoxy sizing. The exact setups for the preparation of nanofiller were reported in our recent paper [21]. Briefly, an aqueous NaOH solution (4.0 mL, 0.1 M) was added to EtOH (50.0 mL). Then HDTMS (4.0 mL) was added into the above solution, and the obtained mixture was ultrasonically dispersed for 10 min. Finally, a sheet-like nanofiller was obtained by removing the EtOH at ambient temperature for 14 days.

The preparation of sizing included the following steps. Firstly, Span-80 and SDS were adopted as emulsifiers and added to the epoxy resin with mechanical stirring of 250 rpm at 55 °C. After mixing, water was added dropwise to obtain an epoxy emulsion used as the film former (Mixture 1 in Fig. 1A). Meanwhile, PEG-MS was added to water under the same magnetic stirring at 60 °C for 1 h, yielding a mixture functioning as the lubricant (Mixture 2 in Fig. 1A). The dissolution of CTAB, acting as an antistatic agent, was accomplished by adding the surfactant into water at 60 °C (Mixture 3 in Fig. 1A). The hydrolysis of the coupling agent was performed by adding KH-550 into the water with pH = 3.0–4.0 (Regulated by glacial acetic acid), and the solution was stirred magnetically until it turned transparent (Mixture 4 in Fig. 1A). The mixture 2–4 were sequentially added to the epoxy emulsion (Mixture 1) with stirring mechanically at a speed of 550 rpm for 1 h. At the end, the synthesized nanofillers were added to the sizing and stirred for another 1 h at 55 °C to obtain the nanocomposite sizing. The sizing was applied on BF surface using a continuous coating system developed in our lab (Fig. 1B) [22]. The traction speed for BF was 2 m/min, and the temperature of two hot air dryers was set both at 120 °C to ensure the spreading of sizing on fiber surface. Finally, BF with nanocomposite sizing was obtained by drying at 120 °C for 2 h.

2.4. Characterization

The tensile strength of single filament was determined by a fiber tensile tester (XQ-1A, New Fiber Instrument Company, Shanghai, China). During the test, the gauge length was set at 25.0 mm, and the tensile speed was 2.0 mm/min according to the standard (ASTM C1557–14). Forty fiber samples were measured and the average value was obtained. An electronic balance with an accuracy of 0.1 mg (ML204T, Mettler Toledo, Switzerland) was used to measure the weight of the fiber, and the mass retention rate (M) was obtained by Eq. 1 [12]:

Table 2
Percentage of elements in BF.

Elements	O	Si	Al	Fe	Ca	Na	Mg	Ti	K
Percentage (wt%)	44.58	23.77	8.43	7.64	6.49	3.62	3.95	0.86	0.54

Table 3
Experimental design of seawater erosion of BF.

Factors	Experimental levels			
	1	2	3	4
A: Immersion temperature (°C)	0	20	40	60
B: Immersion time (Day)	0	5	10	28

Table 4
Experimental schemes of BF exposed to seawater.

Sample No.	A	B	Experimental schemes
1	1	1	A_1B_1
2	1	2	A_1B_2
3	1	3	A_1B_3
4	1	4	A_1B_4
5	2	2	A_2B_2
6	2	1	A_2B_1
7	2	4	A_2B_4
8	2	3	A_2B_3
9	3	3	A_3B_3
10	3	4	A_3B_4
11	3	1	A_3B_1
12	3	2	A_3B_2
13	4	4	A_4B_4
14	4	3	A_4B_3
15	4	2	A_4B_2
16	4	1	A_4B_1

$$M = \frac{M_1}{M_0} \times 100\% \quad (1)$$

Where M_0 and M_1 are the weight of untreated and treated fiber (mg), respectively. The surface morphology of BF was observed using a scanning electron microscope (SEM, Phenom XL, Phenom-World, Netherlands). The distribution of element in fiber was monitored by an energy-dispersive X-ray spectroscope (EDS, X-Flash SDD 5010, Bruker, Germany). Fourier-transform infrared spectroscope (FT-IR, IS50, Thermo Scientific, USA) was used to examine the chemical structure of fiber. BF sample was immersed in simulated seawater at 60 °C for 28 days to study the corrosion resistance of fiber with sizing. After seawater treatment, the sample was washed with water for three times and dried at 105 °C for 1 h.

3. Results and discussions

3.1. Mechanical property of BF

The changes on the tensile strength of BF in simulated seawater were analyzed. Fig. 2A indicates the effect of immersion temperature on the tensile strength of BF. The strength of 20–28, 40–28, and 60–28 samples was 1446 MPa, 1107 MPa and 1038 MPa, respectively. Compared with the untreated fiber (1324 MPa), the strength of the 20–28 sample increased slightly by 9.21%, suggesting that lower temperature had a negligible effect on deteriorating the performance of fiber, and this was possibly due to the reduced stress concentration on fiber surface. With increasing temperature in seawater, saying the samples processed at 40 °C and 60 °C, a significant reduction on the strength of filament was noticed, which could be attributed to the severe damage to the fiber. Notably, the tensile strength of the 20–5 sample reached 1622 MPa, which was 22.51% higher than that of the untreated one. This was due to the exchange of Na^+ in fiber with K^+ in seawater [23]. During this process, the difference in the ion radius (102.0 pm for Na^+ and 138.0 pm for K^+) was accountable for the increased molar volume on fiber surface, thus leading to the compressive stress that could bear the load applied to the fiber. As the temperature was raised, the strength of 40–5 and 60–5 samples was 1416 MPa and 1380 MPa, increased by 6.95% and 4.23% compared with the untreated fiber, respectively. It was speculated that with increasing immersion temperature, more defects were exposed on the fiber surface, which could somehow offset the strength enhancement induced by Na^+/K^+ exchange.

Fig. 2B displays the effect of immersion time on the tensile strength of BF at different temperatures in seawater. The results clearly indicated that the tensile strength of the sample increased at first and then decreased. Compared with the untreated fiber, the tensile strength of 20–5, 20–10, and 20–28 samples was 1622 MPa, 1395 MPa, and 1446 MPa with increasing ratios of 22.51%, 5.36% and 9.21%, respectively. Such enhancement was due to the compressive stress generated by the exchange of Na^+/K^+ on the fiber surface in the initial stage, ultimately hindered by the growing defects as time prolonged. The variation on the strength of BF eroded by the seawater could provide a reference for the long-term application of basalt fiber-reinforced concrete in marine environment.

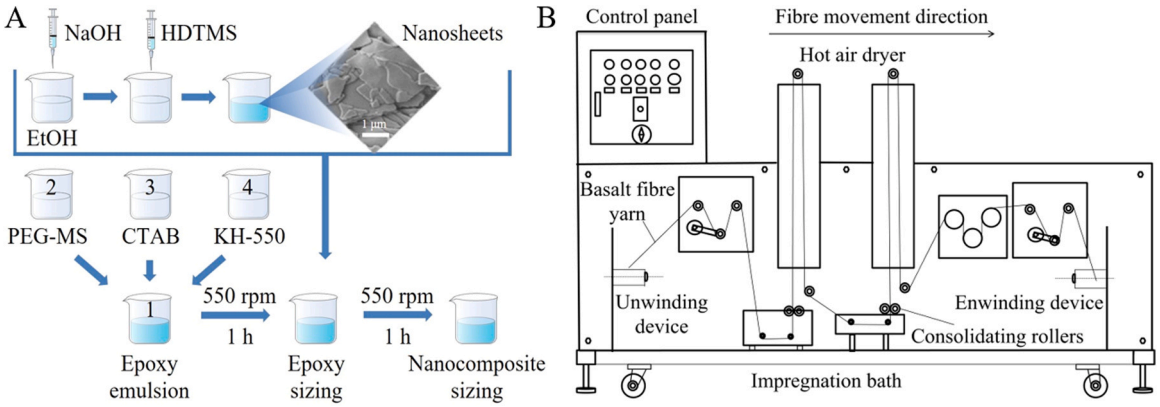

Fig. 1. Schematic showing the preparation of nanocomposite sizing (A) and the facility for the application of sizing on fiber surface (B) [22].

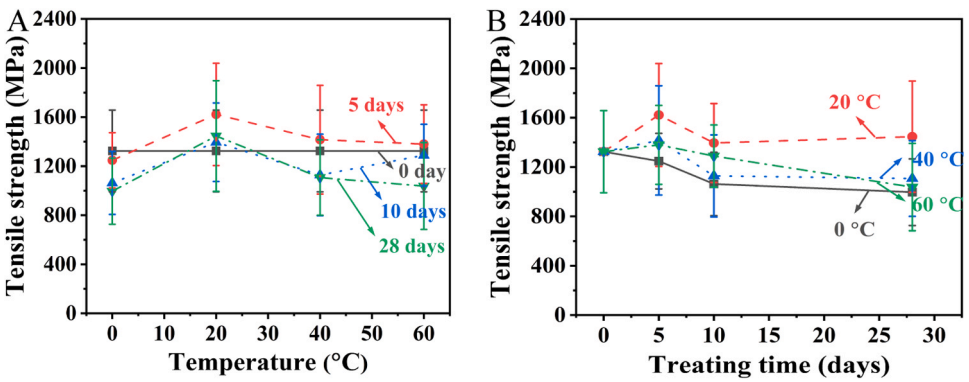

Fig. 2. Variations on the tensile strength of BF with immersion time and temperature after seawater treatment (A: Immersion time; B: Immersion temperature).

3.2. Surface morphology of seawater-corroded BF

Fig. 3 displayed the surface morphology of untreated and seawater-treated BF. The untreated BF had the smooth surface, as shown in Fig. 3A1. When the immersion time for the fiber was same, as the temperature increased from 0 °C to 60 °C, all samples exhibited morphological changes from a smooth surface, then a rougher one with particles, and finally to a multi-scale structure with plate-like particles. For example, only a small number of particles appeared on the surface of 0–28 and 20–28 samples (A4 and B4 in Fig. 3, 28 suggests the days for the immersion). With increasing immersion temperature, a plate-like layer accumulated on fiber surface for the samples of 40–28 and

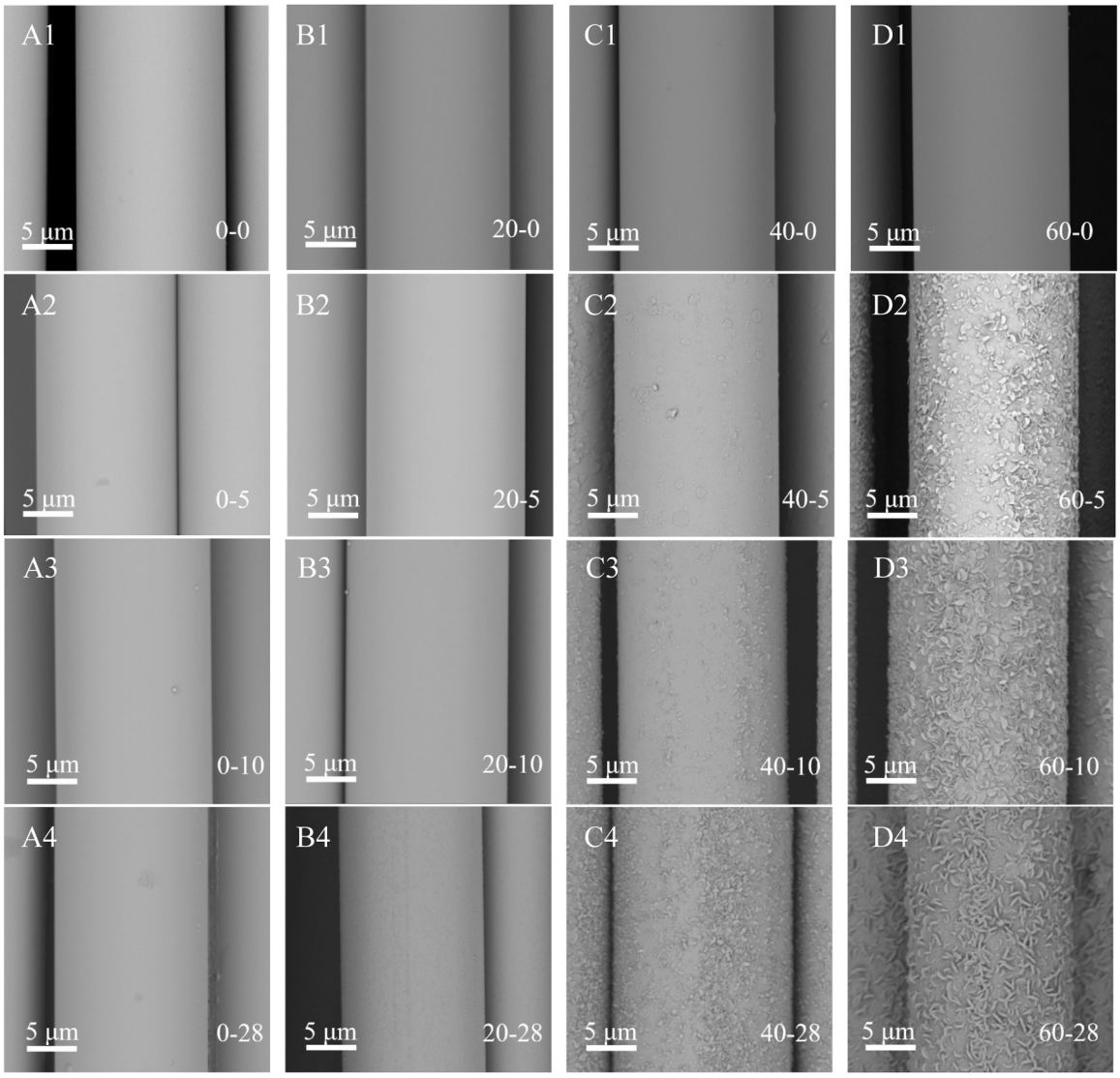

Fig. 3. Morphology of seawater-treated BF under different conditions (A-D: 0 °C, 20 °C, 40 °C, 60 °C; 1–4: 0 day, 5 days, 10 days, 28 days).

60–28 (C4 and D4 in Fig. 3). It was found that the higher the immersion temperature was, the more severe the corrosion of the fiber surface exhibited. In other words, the immersion temperature had a significant effect on the structure integrity of BF in seawater. Besides this observation, when the treatment temperature was same, the variation on the treatment duration led to a similar trend for fiber morphology, as confirmed by the fact that the distribution of the plate-like structures became denser over the time (D2-D4 in Fig. 3). More specifically, with longer immersion time, the thickness of the corrosion layer of 60–5, 60–10, and 60–28 samples increased from 0.37 μm to 0.70 μm. This was accompanied by the augmentation on the size of the plate-like structure on fiber surface from 0.96 μm to 1.70 μm, and the increase on its thickness from 0.08 μm to 0.24 μm, as shown in Fig. 4. Generally, the size and thickness of plate-like structure on the corrosion layer got larger and thicker with time. These results strongly suggested the critical role of the treatment duration on the corrosion behavior of BF in seawater. With consideration on the variation of fiber diameter (Average diameter is 16.04 μm, see Table 1), it could be speculated that the change on the BF diameter before and after seawater treatment was marginal. Anyway, the structures formed on the fiber surface after seawater corrosion may cause stress concentration, further affecting the mechanical performance of fiber and its stability in the practical applications. All in all, it could be concluded that the higher immersion temperature or the longer immersion time could lead to severer corrosion of BF under seawater condition.

In addition, the mass change of bundle BF before and after the seawater treatment was recorded. Interestingly, marginal weight change (<3.0%) on the BF was detected with variations on the immersion temperature and time (A and B in Fig. 5), suggesting the maintenance of the Si-O-Si networks in BF. In other words, although the network modifiers (Na^+, K^+, Ca^{2+}, Mg^{2+}) could leach from the fiber under the seawater and the isolated SiO^- on fiber surface could attract cations in seawater, the newly formed corrosion layer on the filament compensated the mass loss of BF in the previous stage. This assumption was partly supported by the larger and thicker plate-like structure on fiber surface (Fig. 4).

3.3. Seawater corrosion mechanism of BF

The distribution of elements on the cross-section of untreated and seawater-eroded BF was determined qualitatively using an EDS mapping technique. The eight main elements were uniformly distributed according to the results arising from the cross-section view of the untreated BF (Fig. 6A). After seawater treatment, decreased distribution of Si, Fe, Ca, Na, and K around the outer layer of fiber was observed, while the signal from the Mg increased (Fig. 6B). According to the observation on element on fiber cross-section, possible reactions between the seawater and fiber were proposed. Owing to the weak alkaline environment of the seawater, OH^- in the solution could attack the Si-O-Si structure in the fiber, thus forming soluble silicate compounds (Eq. 2). Subsequently, the disintegrated networks in the fiber led to the leaching of Na^+ and K^+ ions, which functioned as network modifiers in the structure of the filament [24]. Furthermore, OH^- could continue reacting with Mg^{2+} in the fiber, generating insoluble hydroxide (Eq. 3) attached to the fiber surface. It is worth noting that the reactions between Cl^- in seawater and Fe^{n+} in fiber were likely to occur, leading to the formation

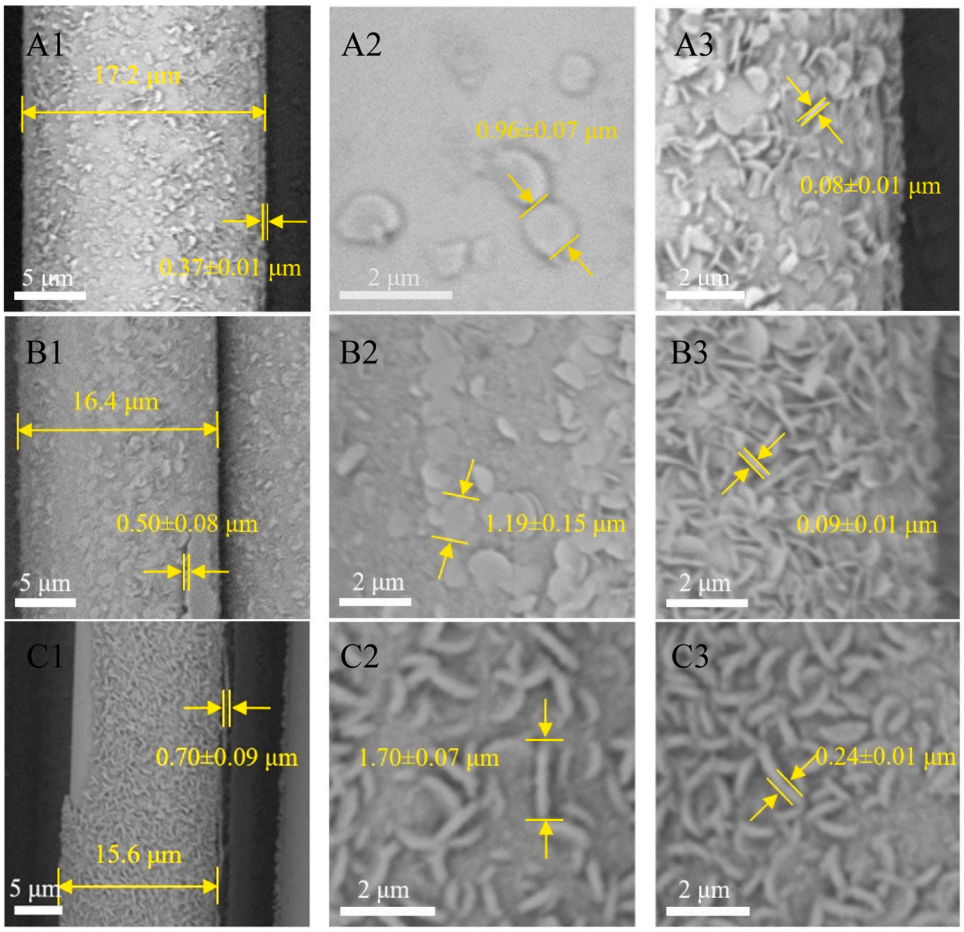

Fig. 4. Size and thickness of the plate-like structure on BF surface (A: 60–5; B: 60–10; C: 60–28; 1: Thickness of corrosion layer; 2: Size of plate-like structure; 3: Thickness of plate-like structure).

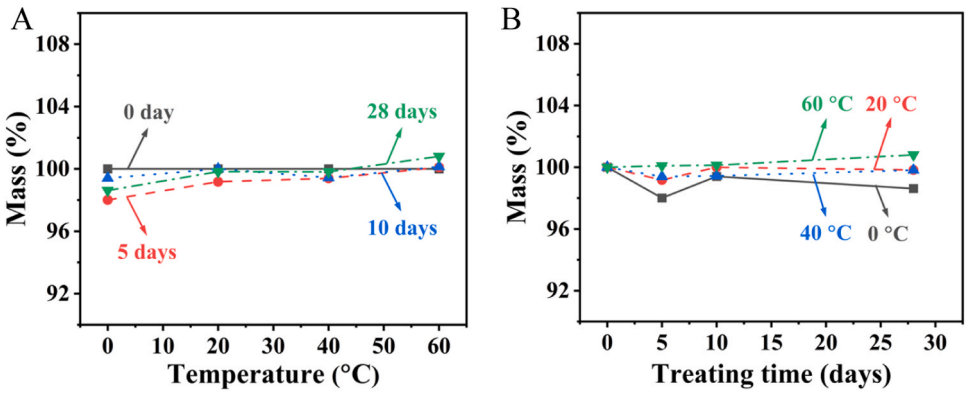

Fig. 5. Variations on the mass of BF with immersion time (A) and temperature (B) after seawater treatment.

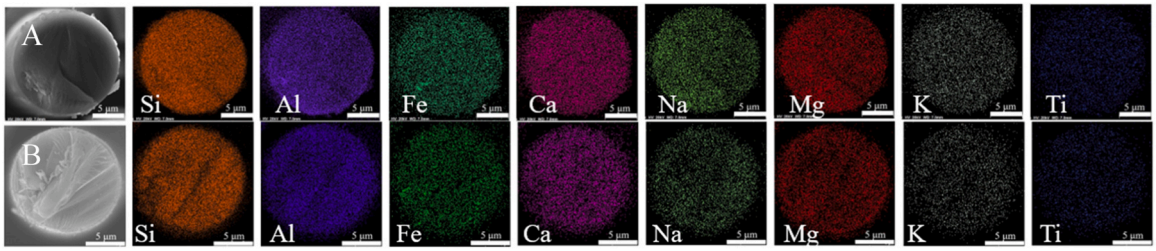

Fig. 6. Distribution of elements on the cross-section of untreated (A) and seawater-eroded (B) BF.

of insoluble hydroxide with the presence of oxygen (Eqs. 4–6) [25].

$$[\text{Si-O-Si}] + \text{OH}^- \rightarrow [\text{Si-O}]^- + [\text{HO-Si}] \quad (2)$$

$$\text{Mg}^{2+} + \text{OH}^- \rightarrow \text{Mg(OH)}_2 \downarrow \quad (3)$$

$$\text{Fe}^{n+} + \text{Cl}^- \rightarrow [\text{FeCl}_n]^{x-} \quad (4)$$

$$[\text{FeCl}_n]^{x-} + \text{OH}^- \rightarrow \text{Fe(OH)}_2 + \text{Cl}^- \quad (5)$$

$$\text{Fe(OH)}_2 + \text{O}_2 + \text{H}_2\text{O} \rightarrow \text{Fe(OH)}_3 \downarrow \quad (6)$$

The effect of seawater erosion on chemical structures of BF was also studied by FT-IR and Raman spectroscopy. For FT-IR spectra (Fig. 7A), the peak at 897 cm^{-1} was identified as stretching vibration of Si-O in the form of $[Si_2O_7]^{6-}$ with a non-bridging oxygen number of 3. The one at 864 cm^{-1} was attributed to stretching vibration of Si-O in $[SiO_4]^{4-}$ with a non-bridging oxygen number of 4. The peaks at 707 cm^{-1} and 658 cm^{-1} were ascribed to stretching vibration of Al-O and Si-O [26], respectively. It was clear that the Si-O-Si/Si-O-Al in the fiber surface was transformed into Si-O/Al-O bond after seawater treatment, thus leading to the increase on the number of non-bridging oxygen and shift of typical peaks to lower wavenumbers. In addition, peaks at 3425 cm^{-1} and 1638 cm^{-1} were assigned to stretching and bending vibrations of O-H [27], originating from the adsorbed water and hydrates on fiber [24]. Peaks in the 1300–1400 cm^{-1} were ascribed to stretching vibrations of M-OH (M = Mg, Fe) [28], indexing to the formation of insoluble metal hydroxides on fiber surface.

As seen from Raman spectra (Fig. 7B), most peaks below 500 cm^{-1} were attributed to vibration of metal oxides in fiber [24]. The peaks at 791 cm^{-1} and 922 cm^{-1} were identified as bending and asymmetric stretching vibration of Si-O structure, which mainly existed in the forms of $[SiO_4]^{4-}$ and $[Si_2O_6]^{4-}$. The one at 1446 cm^{-1} was assigned to CO_3^{2-} vibration in $CaCO_3$ formed by the reaction between $Ca(OH)_2$ and CO_2, while $Ca(OH)_2$ derived from the reaction of Ca^{2+} leached from the fiber and OH^- in seawater, as depicted in Eqs. 7 and 8 [29]. The peaks at 2871 cm^{-1} and 2936 cm^{-1} were attributed to O-H stretching vibrations in $NaCa_2Al_4(CO_3)_4(OH)_8Cl$ (Eqs. 9 and 10) [30] due to the complex interactions of ions in seawater and these originated from the fiber. The EDS mapping, FT-IR and Raman results indicated that plate-like

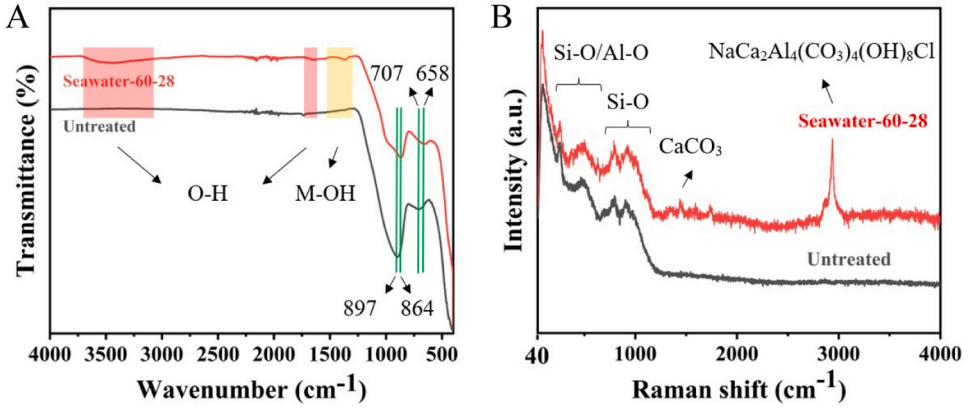

Fig. 7. FT-IR (A) and Raman (B) spectra of the untreated and seawater-eroded BF samples.

structures on the fiber surface were mainly insoluble substances. Compared with Liu's work [14], there was a subtle distinction, for example, plate-like structures were confirmed as $CaCO_3$ and $NaCa_2Al_4(CO_3)_4(OH)_8Cl$ in our study, mainly because the growth process of these structures was different under various seawater conditions.

$$Ca^{2+} + OH^- \rightarrow Ca(OH)_2 \quad (7)$$

$$Ca(OH)_2 + CO_2 \rightarrow CaCO_3 \downarrow \quad (8)$$

$$HCO_3^- + OH^- \rightarrow CO_3^{2-} + H_2O \quad (9)$$

$$Na^+ + Ca^{2+} + Al^{3+} + CO_3^{2-} + OH^- + Cl^- \rightarrow NaCa_2Al_4(CO_3)_4(OH)_8Cl \quad (10)$$

Based on the above findings, a possible mechanism for the corrosion behavior of BF was proposed (Fig. 8). BF was processed in the seawater consisting of multiple cations and anions, such as K^+, Na^+, OH^-, Cl^-, SO_4^{2-}, etc. With the contact between the BF and seawater, the Na^+ in the fiber could be replaced by K^+ in seawater, and the compressive stress generated by the invasion ions was able to enhance the fiber strength. As the seawater treatment continued, OH^- in solution increasingly eroded Si-O-Si structure in fiber. Afterwards, the outer layer of BF began to disintegrate, leading to the leaching of metal ions such as Fe^{n+}. Moreover, OH^- could react with metal ions, such as Mg^{2+}, thus forming a corrosive layer made of insoluble hydroxide on fiber surface. Meanwhile, OH^- could interact with Ca^{2+} and CO_2, forming insoluble $CaCO_3$, which could deposit on fiber surface. The leaching of Ca^{2+} accelerated the destruction of the BF structure. Furthermore, Fe^{n+} in fiber could be attacked by the Cl^- ions in seawater to form some complex chemicals [12], which explained the loss of iron element in BF during the erosion (Fig. 6). Eventually, under the synergistic effect arising from the HCO_3^-, OH^-, Cl^-, Na^+, Ca^{2+}, and Al^{3+} in seawater and fiber, insoluble deposits formed and attached onto the fiber surface. The overall BF erosion in seawater could be described as a dynamic process with competitive reactions, along with variations on fiber strength due to the ion exchange, ion leaching, and the precipitation of insoluble hydroxide on fiber surface. Understanding the degradation mechanism of BF in seawater could provide ideas for developing seawater-resistant BF.

3.4. Corrosion resistance of BF with nanocomposite sizing

Polysilsesquioxane (PSQ) nanosheet with excellent thermal stability was previously reported in our group [21]. Meanwhile, the unique structure and surface property of this nanosheet make it easier to be dispersed in water-based solution, thus showing great potential to be used as a functional filler in sizing for BF (Sizing is a thin and homogenous coating applied on fiber surface during the manufacturing process). The as-synthesized PSQ nanosheet was added into an epoxy-based sizing, and the obtained nanocomposite sizing was applied on fiber surface. Table 5 summarizes the components of commercial and nanocomposite sizing. Compared with the commercial sizing, the nanocomposite one developed in this study featured lowered component contents, and could significantly improve the strength of BF produced in the exactly same conditions. Table 6 lists the tensile strength of BF coated different sizing before and after seawater treatment. The tensile strength of BF with epoxy sizing (1552 MPa) and nanocomposite sizing (1853 MPa) were 17.22% and 39.95% higher than that of BF without sizing (1324 MPa), respectively. Defects were inevitably generated in BF without sizing during the fiber production, leading to the stress concentration on fiber surface. Since the sizing could repair defect structures on fiber surface and reduce the stress concentration [31], the strength of BF with sizing was significantly enhanced, especially for the BF with nanocomposite sizing, as the nanosheets not only filled the voids in the coating layer but also transferred the loaded stress to the fiber.

After seawater treatment at 60 °C for 28 days, all the BF samples displayed a decline in tensile strength. Still, the tensile strength of BF with sizing (1175 MPa) was higher than that of BF without sizing (1038 MPa) due to the isolation effect of the coating on fiber surface towards seawater. Notably, the strength of BF with nanocomposite sizing (1269 MPa) outperformed its counterpart with epoxy sizing owing much to the excellent shielding performance of nanosheet towards solution. The tensile strength of BF with nanocomposite sizing was close to that of untreated fiber in seawater. The reason for this could be explained by the disrupted continuous coating under the addition of

Table 5
Comparison on the components of commercial and nanocomposite sizing.

Components	Film former	Lubricant	Coupling agent	Surfactant	Single fiber strength (MPa)
Commercial sizing*	7.0	1.6	0.8	0.5	1494±392
Nanocomposite sizing	6.0	1.6	0.3	0.2	1853±401

* Note that the exact chemicals used for the formulation of commercial sizing are highly classified by the fiber manufacturer.

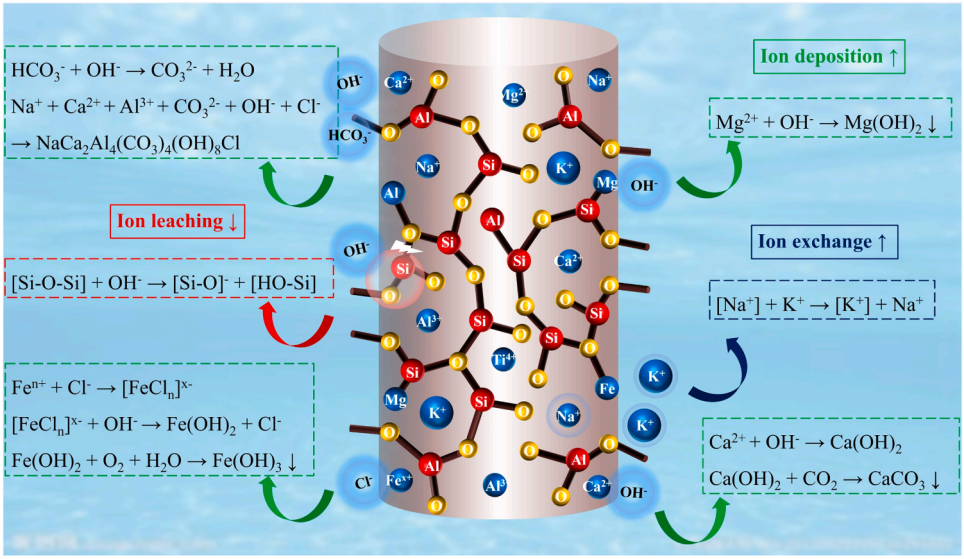

Fig. 8. Schematic illustration showing the erosion mechanism of BF under seawater.

Table 6
Tensile strength of BF after seawater treatment.

Samples	Untreated BF (MPa)	Seawater-treated BF (MPa)
BF without sizing	1324±333	1038±354
BF with epoxy sizing	1552±324	1175±146
BF with nanocomposite sizing	1853±401	1269±235

nanofiller, thus causing the aggravated stress concentration under seawater erosion.

Compared with surface morphologies of BF with different sizing before and after seawater erosion, BF without sizing manifested a smooth surface (A1 in Fig. 9). After coated with sizing, the fiber surface attached the uniform layer (B1 and C1 in Fig. 9). Notably, small protrusions emerged on the fiber in the case of nanocomposite sizing owing to the geometries of nanosheet (C1 in Fig. 9), while BF with epoxy sizing was no protrusions (B1 in Fig. 9). After seawater treatment, newly formed corrosion layers featuring plate-like structures were observed for BF without sizing (A2 in Fig. 9). For the fibers with sizing, both coatings somehow remained after being subjected to the seawater erosion (B2 and C2 in Fig. 9). The retained coating on the cross-section of BF with nanocomposite sizing (Inset C2 in Fig. 9) was more uniform than that of BF with epoxy one (Inset B2 in Fig. 9). These results were also verified by the cross-section SEM images of BF. Although the coating on BF surface was damaged partly during the treatment, the remaining coating prevented further contact between the fiber and seawater, exhibiting improved strength and anti-corrosion performance, as confirmed by the results presented in Table 6.

Based on above discussions, it can be concluded that the nanosheet in nanocomposite sizing played a significant role in regulating the barrier performance of BF to resist erosion of seawater. As displayed in Fig. 10, in the case of BF without sizing, the sample contacted seawater directly, therefore bearing the attacks of OH^- and causing damage to the fiber structure to a maximum extent. For BF with epoxy sizing, the ions in seawater were prone to diffuse and permeate through the sizing before reaching the fiber surface. Remarkably, the ion permeation was largely restrained for BF with nanocomposite sizing since the ions were forced to travel through tortuous and longer paths owing to the presence of nanosheet before contacting with the fiber, which significantly kept the filament from environmental attacks. Therefore, Si-based nanosheet could be an effective sacrificial layer to prevent fiber from being attacked by the OH^- ions in seawater, thereby protecting the integration of fiber structure.

4. Conclusions

In summary, the effect of immersion temperature and time on the tensile strength and morphology of BF exposed to simulated seawater were investigated in this work. The results demonstrated that the tensile strength of BF generally increased at first and then decreased after seawater treatment. Notably, the strength of BF was increased by more than 20% due to the ion exchange between the Na^+ in fiber and K^+ in seawater. The decline on tensile strength of BF was accompanied by the morphological variations with the aggravation of treatment conditions. The fiber surface went through the changes from a smooth surface, then with deposited particles, and to a corrosion layer with plate-like structure. The overall corrosion of BF in simulated seawater can be concluded as a dynamic process, involving several competitive interactions including the fiber strength enhancement arising from ion exchange between Na^+/K^+, deposition of insoluble substances, and the reduced fiber strength due to the damage of Si-O-Si structure. To protect the fiber from corrosion, nanocomposite sizing containing Si-based nanosheet was applied on fiber surface. The anti-corrosion performance of BF towards seawater was improved on account of the barrier and sacrificial effects derived from the nanosheet in the sizing.

The findings of this work shed light on improving the mechanical property of BF. For example, the exchange of small ions (Na^+) in solution with large ones (K^+) on fiber surface can enhance the strength of filament, and this can be conducted with presence of potassium-contained salts in the fiber post-treatment. Besides, developing novel sizing containing two-dimensional nanofillers (Graphene, clay, etc) have the capability to enhance the resistance of BF to chemicals. By harnessing these methods, the strength and surface roughness of BF can be rectified, which is expected to enhance the performance of corresponding fiber-reinforced polymers. The implementation of these ideas will be the topic of our future research.

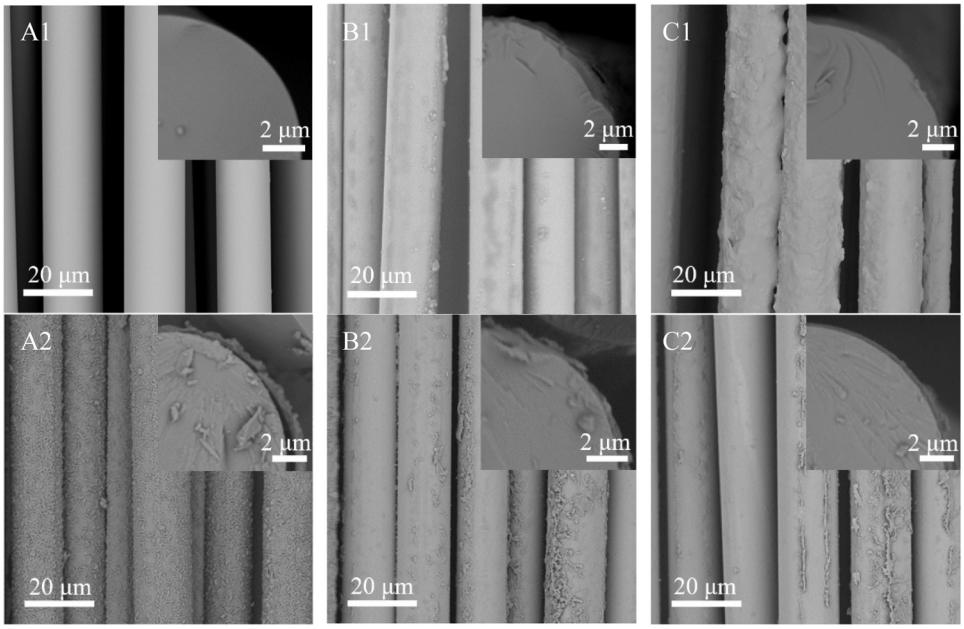

Fig. 9. Morphology of BF before and after seawater treatment (A: Without sizing; B: With epoxy sizing; C: With nanocomposite sizing; 1: Untreated; 2: Seawater-treated; Insets showing the cross-sectional morphology of corresponding sample).

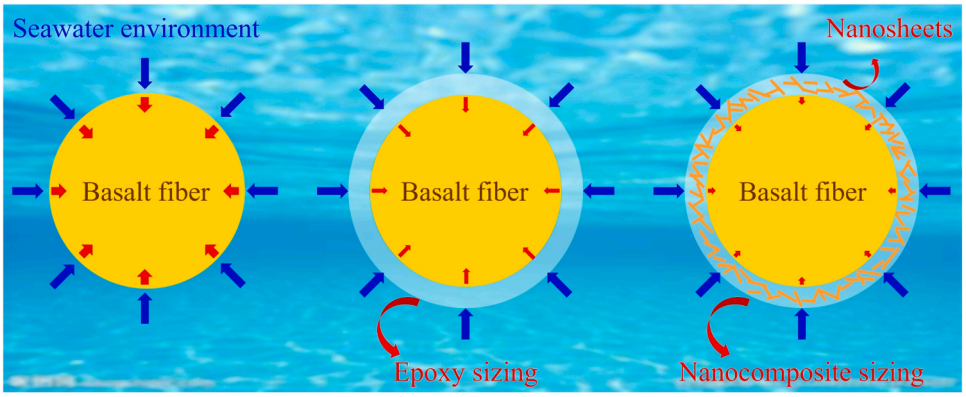

Fig. 10. Schematic showing the corrosion behaviors of BF with different sizing.

CRediT authorship contribution statement

Meng Li: Validation, Investigation, Data Curation, Writing - Original Draft, Visualization, Funding acquisition. **Hui Li:** Writing - Review & Editing, Funding acquisition. **Ghizlane Achagri:** Writing - Review & Editing. **Cun-Guang Liang:** Visualization, Formal analysis. **Molong Duan:** Visualization, Methodology. **Dan Xing:** Visualization, Investigation. **Peng-Cheng Ma:** Conceptualization, Writing - Review & Editing, Supervision, Project administration, Funding acquisition.

Declaration of Competing Interest

The authors declare that they have no known competing financial interests or personal relationships that could have appeared to influence the work reported in this paper.

Acknowledgements

This work was supported by the Scheme of Tianchi Talent on Doctor Introduction in Xinjiang, Talent Program of Chinese Academy of Sciences, and Tianshan Talent Program for Scientific and Technological Innovation in Xinjiang (Grant No.: 2022TSYCLJ0041).

References

[1] G. Feng, Z. Jin, D. Zhu, C. Xiong, Z. Li, X. Wang, Corrosion propagation of steel reinforcement in pre-cracked mortar attacked by seawater using wire beam electrode, Corros. Sci. 208 (2022) 110655, https://doi.org/10.1016/j.corsci.2022.110655.

[2] F. Guo, S. Al-Saadi, R.K. Singh Raman, X.L. Zhao, Durability of fiber reinforced polymer (FRP) in simulated seawater sea sand concrete (SWSSC) environment, Corros. Sci. 141 (2018) 1–13, https://doi.org/10.1016/j.corsci.2018.06.022.

[3] N. Elmessalami, A. El Refai, F. Abed, Fiber-reinforced polymers bars for compression reinforcement: a promising alternative to steel bars, Constr. Build. Mater. 209 (2019) 725–737, https://doi.org/10.1016/j.conbuildmat.2019.03.105.

[4] G. Feng, S. Guo, L. Zhou, W. Luo, X. Guo, Z. Jin, D. Zhu, Effects of surface characteristics and alkalinity on the deterioration of BFRP bars and BFRP-SSC interface in seawater environment, Compos. B. Eng. 268 (2024) 111072, https://doi.org/10.1016/j.compositesb.2023.111072.

[5] X. Wang, G. Wu, Z. Wu, Z. Dong, Q. Xie, Evaluation of prestressed basalt fiber and hybrid fiber reinforced polymer tendons under marine environment, Mater. Des. 64 (2014) 721–728, https://doi.org/10.1016/j.matdes.2014.07.064.

[6] Z. Wang, X.-L. Zhao, G. Xian, G. Wu, R.K. Singh Raman, S. Al-Saadi, A. Haque, Long-term durability of basalt- and glass-fibre reinforced polymer (BFRP/GFRP) bars in seawater and sea sand concrete environment, Constr. Build. Mater. 139 (2017) 467–489, https://doi.org/10.1016/j.conbuildmat.2017.02.038.

[7] M. Lee, K. Kim, C.-W. Chung, W. Kim, Y. Jeong, J. Lee, Mechanical characterization of recycled-PET fiber reinforced mortar composites treated with nano-SiO_2 and mixed with seawater, Constr. Build. Mater. 392 (2023) 131882, https://doi.org/10.1016/j.conbuildmat.2023.131882.

[8] H. Sokairge, F. Elgabbas, A. Rashad, H. Elshafie, Long-term creep behavior of basalt fiber reinforced polymer bars, Constr. Build. Mater. 260 (2020) 120437, https://doi.org/10.1016/j.conbuildmat.2020.120437.

[9] J. Shi, S. Sun, X. Cao, H. Wang, Pullout behaviors of basalt fiber-reinforced polymer bars with mechanical anchorages for concrete structures exposed to seawater, Constr. Build. Mater. 373 (2023) 130866, https://doi.org/10.1016/j.conbuildmat.2023.130866.

[10] S. Selcuk, U. Ahmetoglu, E.C. Gokce, Basalt fiber reinforced polymer composites (BFRP) other than rebars: a review, Mater. Today Commun. 37 (2023) 107359, https://doi.org/10.1016/j.mtcomm.2023.107359.

[11] J. Shi, X. Wang, L. Ding, Z. Wu, Degradation of creep behaviors of basalt fiber-reinforced polymer tendons in salt solution, J. Mater. Civ. Eng. 30 (12) (2018) 04018317, https://doi.org/10.1061/(ASCE)MT.1943-5533.0002525.

[12] P. Cousin, M. Hassan, P. Vijay, M. Robert, B. Benmokrane, Chemical resistance of carbon, basalt, and glass fibers used in FRP reinforcing bars, J. Compos. Mater. 53 (26-27) (2019) 3651–3670, https://doi.org/10.1177/0021998319844306.

[13] Z.Y. Lu, M.C. Jiang, Y.F. Pan, G.J. Xian, M.M. Yang, Durability of basalt fibers, glass fibers, and their reinforced polymer composites in artificial seawater, Polym. Compos. 43 (4) (2022) 1961–1973, https://doi.org/10.1002/pc.26511.

[14] B. Ding, L. Zhang, J. Liu, The difference in weather resistance and corrosion process for different types of basalt fiber, J. Non Cryst. Solids 590 (2022) 121678, https://doi.org/10.1016/j.jnoncrysol.2022.121678.

[15] Y.V. Lipatov, S.I. Gutnikov, M.S. Manylov, B.I. Lazoryak, Effect of ZrO_2 on the alkali resistance and mechanical properties of basalt fibers, Inorg. Mater. 48 (7) (2012) 751–756, https://doi.org/10.1134/S0020168512060106.

[16] Y.V. Lipatov, S.I. Gutnikov, B.I. Lazoryak, Zr-rich basalt continuous fibers with increased alkali resistant properties, Constr. Build. Mater. 288 (2021) 123089, https://doi.org/10.1016/j.conbuildmat.2021.123089.

[17] H. Dou, J. Bai, H. Lu, T. Zhang, L. Kong, Z. Bai, W. Li, Effect of TiO_2 on preparation condition, mechanical properties and alkali resistance of continuous basalt fibers, Cem. Concr. Compos. 136 (2023) 104861, https://doi.org/10.1016/j.cemconcomp.2022.104861.

[18] J.-W. Shi, H. Zhu, J.-G. Dai, X. Wang, Z.-S. Wu, Effect of rubber toughening modification on the tensile behavior of FRP composites in concrete-based alkaline environment, J. Mater. Civ. Eng. 27 (12) (2015) 04015054, https://doi.org/10.1061/(ASCE)MT.1943-5533.0001331.

[19] P.-C. Ma, J.-W. Liu, S.-L. Gao, E. Mäder, Development of functional glass fibres with nanocomposite coating: a comparative study, Compos. Part A Appl. Sci. Manuf. 44 (2013) 16–22, https://doi.org/10.1016/j.compositesa.2012.08.027.

[20] M.-Y. Liu, H.-G. Zhu, N.A. Siddiqui, C.K.Y. Leung, J.-K. Kim, Glass fibers with clay nanocomposite coating: improved barrier resistance in alkaline environment, Compos. Part A Appl. Sci. Manuf. 42 (12) (2011) 2051–2059, https://doi.org/10.1016/j.compositesa.2011.09.013.

[21] M. Li, B. Hao, L. Zhang, H. Li, P. Lv, X. Yue, A. Yasin, P.-C. Ma, Facile preparation of a polysilsesquioxane sheet with a three-dimensional structure, Mater. Chem. Front. 5 (19) (2021) 7176–7183, https://doi.org/10.1039/D1QM00785H.

[22] D. Xing, X.-Y. Xi, M.-G. Qi, Q.-B. Zheng, P.-C. Ma, Optimization on the formulation of sizing to enhance the mechanical properties of basalt fiber, J. Text. Inst. 112 (4) (2020) 1–11, https://doi.org/10.1080/00405000.2020.1771078.

[23] M. Wang, B. Wang, N.M.A. Krishnan, Y. Yu, M.M. Smedskjaer, J.C. Mauro, G. Sant, M. Bauchy, Ion exchange strengthening and thermal expansion of glasses: common origin and critical role of network connectivity, J. Non Cryst. Solids 455 (2017) 70–74, https://doi.org/10.1016/j.jnoncrysol.2016.10.027.

[24] D. Xing, X.-Y. Xi, P.-C. Ma, Factors governing the tensile strength of basalt fibre, Compos. Part A Appl. Sci. Manuf. 119 (2019) 127–133, https://doi.org/10.1016/j.compositesa.2019.01.027.

[25] B. Wei, H. Cao, S. Song, Degradation of basalt fibre and glass fibre/epoxy resin composites in seawater, Corros. Sci. 53 (1) (2011) 426–431, https://doi.org/10.1016/j.corsci.2010.09.053.

[26] X. Li, H. Guo, Tunable Bi near-infrared emission in aluminosilicate glass based on local excess charge model, J. Chin. Ceram. Soc. 50 (4) (2022) 902–912, https://doi.org/10.14062/j.issn.0454-5648.20211023.

[27] F. Li, G. Li, H. Wang, Q. Tong, Effect of acid/alkali corroison on properties of basalt fiber yarn, Mater. Rep. 29 (2) (2015) 110–113.

[28] V.A. Rybin, A.V. Utkin, N.I. Baklanova, Alkali resistance, microstructural and mechanical performance of zirconia-coated basalt fibers, Cem. Concr. Res. 53 (2013) 1–8, https://doi.org/10.1016/j.cemconres.2013.06.002.

[29] M.L. Frezzotti, F. Tecce, A. Casagli, Raman spectroscopy for fluid inclusion analysis, J. Geochem. Explor. 112 (2012) 1–20, https://doi.org/10.1016/j.gexplo.2011.09.009.

[30] R.L. Frost, M. Dickfos, Hydrated double carbonates - a Raman and infrared spectroscopic study, Polyhedron 26 (15) (2007) 4503–4508, https://doi.org/10.1016/j.poly.2007.06.003.

[31] J.L. Thomason, Glass fibre sizing: a review, Compos. Part A Appl. Sci. Manuf. 127 (2019) 105619, https://doi.org/10.1016/j.compositesa.2019.105619.